Is the $7/2_1^-$ Isomer State of ^{43}S Spherical?

R. Chevrier,[1] J. M. Daugas,[1] L. Gaudefroy,[1] Y. Ichikawa,[2] H. Ueno,[2] M. Hass,[3] H. Haas,[4] S. Cottenier,[5] N. Aoi,[6] K. Asahi,[7] D. L. Balabanski,[8] N. Fukuda,[2] T. Furukawa,[9] G. Georgiev,[10] H. Hayashi,[7] H. Iijima,[7] N. Inabe,[2] T. Inoue,[7] M. Ishihara,[2] Y. Ishii,[7] D. Kameda,[2] T. Kubo,[2] T. Nanao,[7] G. Neyens,[11] T. Ohnishi,[2] M. M. Rajabali,[11] K. Suzuki,[7] H. Takeda,[2] M. Tsuchiya,[7] N. Vermeulen,[11] H. Watanabe,[2] and A. Yoshimi[12]

[1]*CEA, DAM, DIF, F-91297 Arpajon, France*
[2]*RIKEN Nishina Center, 2-1 Hirosawa, Wako, Saitama 351-0198, Japan*
[3]*Department of Particle Physics, Weizmann Institute of Science, Rehovot 76100, Israel*
[4]*CERN/PH-IS, 1211 Geneve-23, Switzerland*
[5]*Center for Molecular Modeling, Department of Materials Science and Engineering, Ghent University, Technologiepark 903, BE-9052 Zwijnaarde, Belgium*
[6]*Research Center for Nuclear Physics, Osaka University, Ibaraki, Osaka 567-0047, Japan*
[7]*Department of Physics, Tokyo Institute of Technology, 2-12-1 Oh-okayama, Meguro-ku, Tokyo 152-8551, Japan*
[8]*Institute for Nuclear Research and Nuclear Energy, Bulgarian Academy of Sciences, 1784 Sofia, Bulgaria*
[9]*Department of Physics, Tokyo Metropolitan University, 1-1 Minami-Osawa, Hachioji-shi, Tokyo 192-0397, Japan*
[10]*CSNSM, CNRS/IN2P3, 91405 Orsay-Campus, France*
[11]*Instituut voor Kern-en Stralingsfysica, K U Leuven, B-3001 Leuven, Belgium*
[12]*Research Core for Extreme Quantum World, Okayama University, Okayama 700-8530, Japan*

(Received 13 December 2011; published 16 April 2012)

We report on the spectroscopic quadrupole moment measurement of the $7/2_1^-$ isomeric state in $^{43}_{16}S_{27}$ [$E^* = 320.5(5)$ keV, $T_{1/2} = 415(3)$ ns], using the time dependent perturbed angular distribution technique at the RIKEN RIBF facility. Our value, $|Q_s| = 23(3)\ e\text{fm}^2$, is larger than that expected for a single-particle state. Shell model calculations using the modern SDPF-U interaction for this mass region reproduce remarkably well the measured $|Q_s|$, and show that non-negligible correlations drive the isomeric state away from a purely spherical shape.

DOI: 10.1103/PhysRevLett.108.162501 PACS numbers: 21.60.Cs, 21.10.Ky, 23.35.+g

Thanks to recent developments of intense radioactive beams, unexplored landscapes of the Ségré chart such as the structure of nuclei far from the stability line can now be investigated in detail. One of the most striking results from the two last decades is the modification or disappearance of the so-called ''magic numbers'' in exotic nuclei. The first evidence for such structure modification was observed in $N = 20$ neutron-rich nuclei [1]. Similar information has been found for exotic nuclei around $N = 28$ [2]. For the latter nuclei, the set of available theoretical [3,4] and experimental [5–9] data provide a coherent description of the gradual erosion of the $N = 28$ gap and the onset of deformation from the spherical ^{48}Ca nucleus towards the neutron-rich and oblate deformed ^{42}Si nucleus [10]. Midway from these two extremes lie the sulfur isotopes of transitional nature, for which spherical or deformed shape coexistence is expected in ^{43,44}S mainly based on theoretical interpretations of recent experimental data [11,12]. However, no definitive experimental evidence assess shape coexistence in these isotopes. Within the shell model (SM) framework, shape transitions in this mass region reflect the strong increase of correlation energy while moving away from the stability line [13,14]. From a recent interpretation of in-beam γ-ray spectroscopy data in exotic Si isotopes, the aforementioned increase of the correlation energy was mainly ascribed to proton-neutron interactions [15]. The latter would be responsible for the inversion between *natural* (i.e., rather spherical) and *intruder* (i.e., deformed) configurations in both ^{43,44}S. For the ^{43}S isomeric state [$E^* = 320.5(5)$ keV, $T_{1/2} = 415(4)$ ns], the spin-parity $J^\pi = 7/2^-$ resulting from the natural orbital configuration $(\nu f_{7/2})^{-1}$ can be inferred from the very good agreement of SM calculations with the recently measured magnetic moment [$g^{\text{exp}} = -0.317(4)$, $g^{\text{SM}} = -0.280$] [12]. The SM furthermore predicts that this normal configuration coexists with the intruder prolate deformed $3/2^-$ ground state (g.s.).

In order to verify this scenario in ^{43}S, two experimental observations are still missing: (i) evidence for the rotational band built on top of the suspected intruder prolate ground state of the nucleus and (ii) determination of the rather spherical nature of the isomeric state. In this Letter we report on the measurement of the spectroscopic quadrupole moment of the $7/2_1^-$ isomeric state using the TDPAD technique [16] on spin-aligned nuclei produced from an in-flight ^{43}S fragment beam [17–21]. The results suggest that correlations drive the isomeric state away from a purely spherical shape.

The TDPAD method was applied on spin-aligned ^{43m}S produced via the fragmentation of a ^{48}Ca beam at both high intensity (4 μeA) and energy ($345A \cdot$ MeV). The primary beam impinged on a 4-mm thick ^{9}Be target, located at the

entrance of the BigRIPS spectrometer at the RIKEN RIBF facility in Japan [22]. The fully stripped fragments were selected through the spectrometer using a 15-mm thick Al achromatic degrader placed at the intermediate dispersive plane. Since the fragments' time of flight was ≈ 430 ns in the nuclear frame, $\approx 50\%$ of the produced ^{43}S isomers reached the detection system located at the focal plane of the spectrometer at about 70 m from the production target. They were slowed down by a 10-mm thick Al degrader and implanted in an appropriate host material. A 0.1-mm thick plastic scintillator, located 1.5 m upstream from the host, provided a start signal for the TDPAD measurement and was used to monitor the implantation rate ($\approx 8 \times 10^3$ out of 1.5×10^4 implanted fragments per second were ^{43}S nuclei) and to determine the ion arrival time. The g factor of ^{43m}S was first measured in order to validate the method and to perform the momentum selection where the spin-alignment was the highest. ^{43m}S fragments were selected both in the center and the outermost wing of the longitudinal momentum distribution, and implanted in an annealed 3-mm thick Cu host placed between the poles of an electromagnet providing a static magnetic field $\vec{B}$ in the vertical direction with a strength $B = 0.670(1)$ T. It was used to induce a Larmor precession of the spin-aligned ^{43m}S fragments. The 320.5 keV γ-ray deexciting the isomer was recorded with four high-purity germanium detectors (HPGe), placed in the horizontal plane around the host at 45° with respect to the beam axis and 90° with respect to each other. Time and energy information were collected on an event-by-event basis. By gating on the 320.5 keV $E2(7/2^-_1 \rightarrow 3/2^-_{g.s.})$ decay transition, the time spectrum of each detector was used to generate the ratio $R(t)$:

$$R(t) = \frac{I_{34}(\theta = \pm 45°, t) - \epsilon I_{12}(\theta = \pm 135°, t)}{I_{34}(\theta = \pm 45°, t) + \epsilon I_{12}(\theta = \pm 135°, t)}, \quad (1)$$

where I_{ij} is the sum of the photopeak intensities in Ge detectors i and j, θ is the detection angle with respect to the beam axis, and ϵ is a normalization coefficient. The measured decay time of the $7/2^-_1$ isomeric state yields a half-life of 415(3) ns. Figure 1 displays the $R(t)$ functions for fragments selected (a) in the center and (b) in the wing of the momentum distribution. The amplitude of each oscillation is related to the amount of spin alignment of the fragments [17]. In this case, the optimum alignment is achieved in the center of the momentum distribution with a value of $+8.1(9)\%$. When selected in the outermost wing of the momentum distribution, the fragments exhibit an alignment of $-2.8(6)\%$, limiting the accuracy in determining the g- factor. The g factor extracted from the data set reported in Fig. 1(a) amounts to $-0.312(12)$, in agreement with that reported in Ref. [12]. Knowing g, one can determine the angle α [19] of the spin-orientation axis (Z_{OR}) (i.e., the symmetry axis of the spin-aligned ensemble) with respect to the beam axis at the implantation position. The

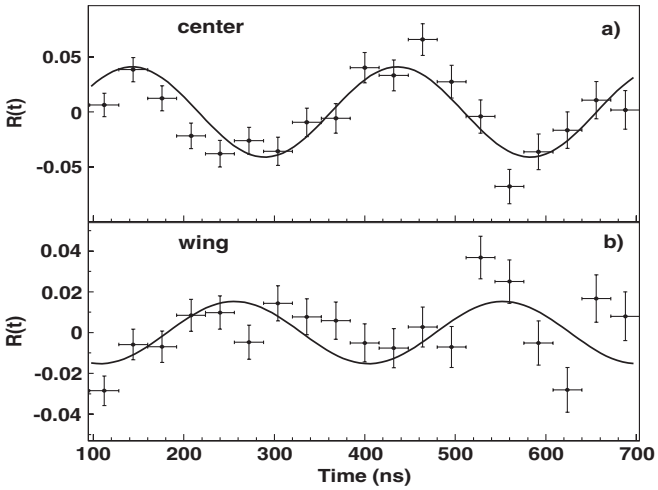

FIG. 1. $R(t)$ function for the $E2(7/2^-_1 \rightarrow 3/2^-_{g.s.})$ transition in the case of fragments selected at (a) the center and (b) the outermost wing of the momentum distribution.

angle is given by $\alpha = -\theta_c(1 - \frac{gA}{2Q})$, with $\theta_c = 60°$ the angle between the ^{43}S secondary beam at the target position and at the implantation position, A and Q the mass number and the charge state (here $Q = Z$) of the selected fragment. We find $\alpha = 86°$.

For the quadrupole moment measurement, fragments were implanted in a pyrite (FeS_2) single crystal host, providing an electric field gradient (EFG) V_{zz}. Fe atoms occupy a face-centered cubic sublattice in which sulfur atoms are grouped as S_2 dimers directed along $\langle 111 \rangle$ directions [23]. Consequently, the EFG has four components oriented along $\langle 111 \rangle$ axes at the sulfur positions. By orienting any of the three major axis $\langle 100, 001, \text{ or } 010 \rangle$ along the beam one ($\langle 010 \rangle$ in present case), the four EFG components make an angle of $\sim 55°$ with respect to the beam and chosen axes. The highest anisotropy is found when gamma detectors are set perpendicular to the beam direction, as shown in Fig. 2.

The photopeak intensities used in Eq. (1) are $I_i(t) = I_0 e^{-t/\tau} W(\theta_i, \phi_i, t)$, where θ_i and ϕ_i are the angles in spherical coordinates of detector i with respect to the laboratory reference frame, I_0 the photopeak intensity at

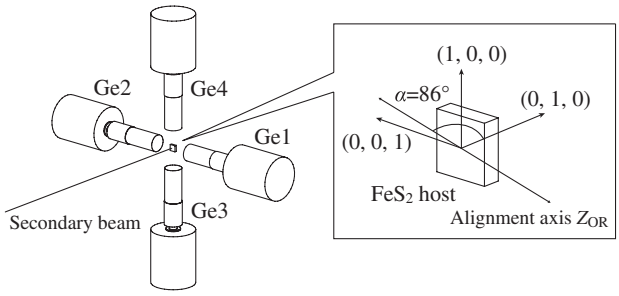

FIG. 2. Schematic view of the experimental setup for the quadrupole moment measurement.

$t = t_0$, and τ the lifetime of the isomeric state. The perturbed angular distribution $W(\theta_i, \phi_i, t)$ is defined by perturbation coefficients, which consist of a superposition of harmonics with basic frequency $\omega_0 = \frac{6*2\pi\nu_Q}{4J(2J-1)}$, where ν_Q is the quadrupole frequency [24]. The spectroscopic quadrupole moment Q_s can be deduced from the quadrupole frequency as $Q_s = \nu_Q h/eV_{zz}$. The $R(t)$ function is displayed in Fig. 3. A χ^2-minimization procedure was used to determine the parameters and their statistical errors. The free parameters in the fit were the amplitude, ν_Q and t_0. Since the sign of Q_s is only accessible with a spin-polarized nuclear ensemble, only the absolute value was extracted. The value of the quadrupole frequency obtained is $\mid \nu_Q(^{43}\mathrm{S}, 7/2_1^-) \mid = 76(3)$ MHz. The amount of alignment is $+2.6(6)\%$, which corresponds to 32% of the alignment observed in the g-factor measurement for a similar selection of the momentum distribution. Possible reasons for such a reduction are that not all ^{43m}S fragments are implanted in a sulfur site in the FeS_2 host and there exist complex four EFG components in the crystal.

In order to determine the spectroscopic quadrupole moment $\mid Q_s \mid$ from $\mid \nu_Q \mid$, one has to know the value of the EFG at a sulfur nucleus site in a FeS_2 crystal. We adopt this value from *ab initio* calculations within the framework of density functional theory [25–27], as implemented in the WIEN2K package [28] for periodic solids. A similar procedure as used in Refs. [29–31] is applied using the technical settings reported in Ref. [32]. The numerical convergence of present calculations was carefully verified. We obtain an EFG at the Fe nucleus of -3.65×10^{-21} V/m^2, which can be checked against an experimental value of -3.75×10^{-21} V/m^2 [33]. This gives confidence that the EFG for S, $+14.14 \times 10^{-21}$ V/m^2, obtained by the same calculation, is reliable as well. Using this value, the spectroscopic quadrupole moment of the $7/2_1^-$ isomer in ^{43}S is $\mid Q_s(^{43}\mathrm{S}, 7/2_1^-) \mid = 23(3)$ $e$fm^2.

Shell model calculations were performed using the ANTOINE code [34,35] and the SDPF-U interaction [36] within the full $sd(fp)$ valence space for protons (neutrons) to compare with our result. Values for the effective charges $e_\pi = 1.35e$, $e_\nu = 0.35e$, and g factors $g_l^\pi = 1.1$, $g_s^\pi = 4.1895$, $g_l^\nu = -0.1$, $g_s^\nu = -2.8695$ [36] were used for protons and neutrons, respectively, in order to estimate electromagnetic properties. The present theoretical approach using the same interaction has already been shown to provide a fairly good description of the evolution of the nuclear structure from the stability line toward exotic neutron-rich nuclei at $N = 27$, 28, and 29 [9–12,14,15,36,37]. The calculated level scheme for ^{43}S, restricted to states of interest here, is shown in Fig. 4. We note that the calculated excitation energy of the $7/2_1^-$ state ($E^* = 728$ keV) is overestimated by about 400 keV. This deviation could be ascribed to an underestimation of the binding energy of the isomeric state or an overestimation of the binding energy of the ground state. The calculated spectroscopic quadrupole moment of the $7/2_1^-$ isomer is $Q_s^{\mathrm{SM}} = +25$ $e$fm^2, in remarkable agreement with the measured value. It is significantly larger than that expected for a single hole in the $\nu f_{7/2}$ orbit, which is $Q_{s.p.} \simeq 4$ $e$fm^2. The latter was estimated from the simple relation $Q_{s.p.} = -e_j \frac{2j-1}{2j+2}\langle r_j^2 \rangle$, where $e_j = 0.35e$ stands for the effective charge of the unpaired neutron lying in the $f_{7/2}$ orbit, and $\langle r_j^2 \rangle = 17$ fm^2 is the mean square radius for that orbit estimated using the wave function (WF) obtained from a Wood-Saxon potential with standard parameters. This single-particle limit is in perfect agreement with that calculated within the present SM approach for ^{47}Ca [$Q_s^{\mathrm{SM}}(^{47}\mathrm{Ca}_{g.s.}) = 3.9$ $e$fm^2]. The origin of the increased ^{43}S quadrupole moment is addressed in the following, using SM calculations.

Among the states calculated above the isomer, only the $9/2_1^-$ state shows strong electromagnetic transitions to the $7/2_1^-$ state (see Fig. 4). The reduced transition probabilities between higher angular momentum states and both the

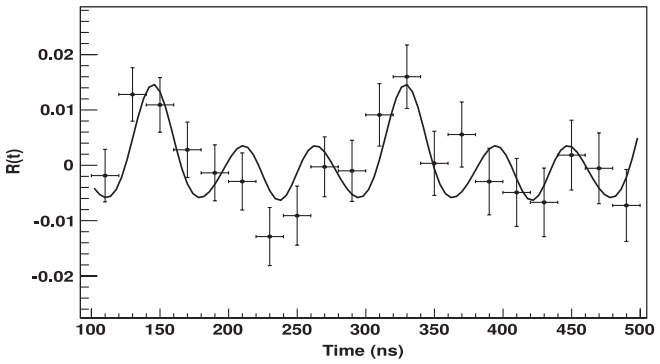

FIG. 3. $R(t)$ function for the $E2(7/2_1^- \rightarrow 3/2_{g.s.}^-)$ transition deexciting the $7/2_1^-$ isomer.

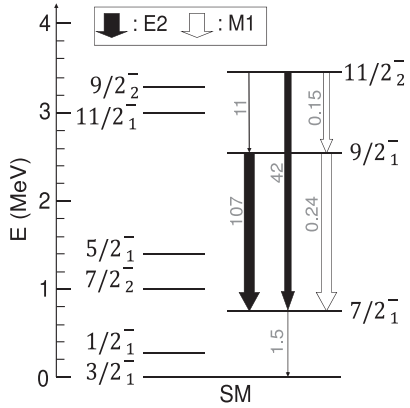

FIG. 4. Predicted low-lying level scheme for ^{43}S. The left side displays the predicted rotational band built on top of the ground state [12]. Transition probabilities [in e^2 fm^4 (μ_N) for $E2$ ($M1$) transitions] are reported along the arrows.

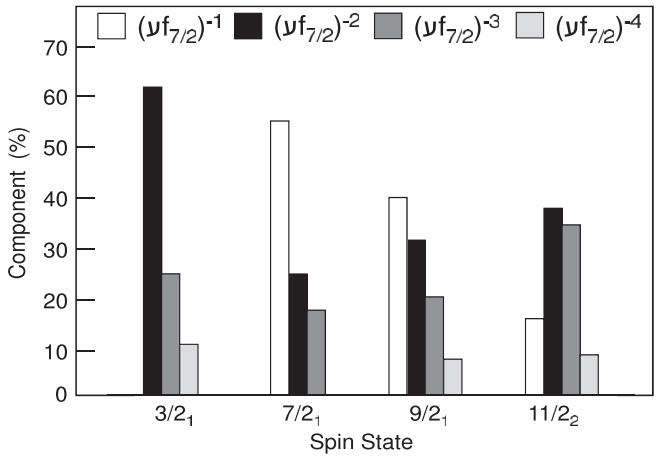

FIG. 5. Percentage of natural $(\nu f_{7/2})^{-1}$ and intruder $(\nu f_{7/2})^{-2,-3,-4}$ neutron configurations in the wave functions of states of interest. Components contributing less than 5% are not represented.

$7/2_1^-$ and $9/2_1^-$ states are weaker than those between the two latter states (see Fig. 4 for the $11/2_2^-$). Therefore, present SM calculations do not show a clear indication for deformed structure built on top of the $7/2_1^-$ isomer.

In order to get a better understanding of the structure of the isomer and higher lying states reported in Fig. 4, their WFs have been decomposed in terms of *natural* and *intruder* neutron configurations. The former corresponds to a single hole in the $\nu f_{7/2}$ orbit, while the latter correspond to configurations for which at least one neutron has been promoted from the $\nu f_{7/2}$ orbit toward higher fp orbits. The results of the decomposition are displayed in Fig. 5.

The ground state neutron WF of ^{43}S is dominated by intruder configurations, the natural one contributing less than 1%. We note that states belonging to the ground state rotational band predicted in that nucleus [12] exhibit similar WF decompositions. Experimentally the $7/2_2^-$ state has been identified as a rotational state [38,39]. A more detailed description of the corresponding WFs in terms of proton and neutron components is shown in Fig. 7 of Ref. [37]. The natural neutron configuration $(\nu f_{7/2})^{-1}$ is the most prominent for the $7/2_1^-$ isomer (53%). However, intruder neutron configurations account for the rest of the neutron WF (i.e., 47%), most of which correspond to one and two neutron excitations across the $N = 28$ shell gap (see Fig. 5). The natural neutron configuration is also found in higher lying states considered here, but its contribution gradually decreases while moving higher in excitation energy. Already for the $9/2_1^-$ state, the contribution of the $(\nu f_{7/2})^{-1}$ configuration is less than those from intruder configurations. The difference between the WF of the isomer state and the WFs of the states lying above the isomer corroborate the absence of deformed structure in these states. The non-negligible contribution of intruder configurations to the neutron WF of the isomer reflects the relatively large amount of multipole energy (i.e., correlation energy) contributing to the total energy of the isomer (see Ref. [14] for a detailed study in this mass region). Indeed, for the well-correlated ground state of the nucleus, the correlation energy amounts to about 16 MeV, while for the $7/2_1^-$ isomer, it amounts to 13 MeV. These values should be compared to that found in Ca isotopes around $N = 28$ of about 2 MeV. As recently shown, proton-neutron correlations give a large contribution to these values of correlation energy [15]. The latter induces non-negligible configuration mixing in the WF of the isomer responsible for the departure of its spectroscopic quadrupole moment from the single-particle limit.

In summary, we report on the measurement of the quadrupole moment of the $7/2_1^-$ isomer in ^{43}S using the TDPAD method on spin-aligned fragments selected through the BigRIPS separator at RIKEN. The measured spectroscopic quadrupole moment, $|\,Q_s(^{43}\mathrm{S}, 7/2^-)\,| = 23(3)\ e\mathrm{fm}^2$, is significantly larger than that expected for a single-particle state. Shell model calculations reproduce remarkably well our experimental value. Within this approach, no deformed structure is found on top of the isomer. Although the natural neutron configuration $(\nu f_{7/2})^{-1}$ is prominent in the wave function of the isomer, SM calculations show that intruder neutron configurations arising from proton-neutron correlations have a non-negligible impact on the structure of this state. In particular, intruder configurations are understood to be reason behind the relatively large quadrupole moment reported for that state. *Sensu stricto*, the studied isomer in ^{43}S cannot be regarded as a spherical state. However, while correlations are at play for this state, they are not developed enough to drive the state towards deformation since no deformed structure is predicted on top of it. Therefore the properties of the $7/2_1^-$ isomer in ^{43}S are understood as a remnant effect of the eroding $N = 28$ shell closure. In order to give unambiguous evidence of shape coexistence in the low-lying structure of ^{43}S, it would be of great interest to experimentally identify the states belonging to the predicted rotational band built on top of the ground state.

The authors are thankful to the staff at RIBF at RIKEN and to T. Ahn for reading the manuscript. The experiment was performed under Program No. NP0906-RIBF06 at RIBF, operated by RIKEN Nishina Center and CNS, the University of Tokyo. This work was supported by the Japanese-French Hubert Curien partnership (PHC), implemented by the Japanese Society for the Promotion Science (JSPS) and the French Ministère de l'Enseignement Superieur et de la Recherche (MESR) et des Affaires Etrangères et Européennes (MAEE), the BriX IAP P6/23 project of OSTC Belgium, the Grant-in Aid for Scientific Research (No. 20532089) of Japan, and the Bulgarian National Science Fund, Grants No. DID-02/16 and No. DRNF-02/5.

[1] C. Détraz, D. Guillemaud, G. Huber, R. Klapisch, M. Langevin, F. Naulin, C. Thibault, L. C. Carraz, and F. Touchard, Phys. Rev. C **19**, 164 (1979).
[2] O. Sorlin and M.-G. Porquet, Prog. Part. Nucl. Phys. **61**, 602 (2008).
[3] V. E. Oberacker, A. S. Umar, E. Terán, and A. Blazkiewicz, Phys. Rev. C **68**, 064302 (2003).
[4] S. Peru, M. Girod, and J. F. Berger, Eur. Phys. J. A **9**, 35 (2000).
[5] O. Sorlin *et al.*, Phys. Rev. C **47**, 2941 (1993).
[6] F. Sarazin *et al.*, Phys. Rev. Lett. **84**, 5062 (2000).
[7] P. Himpe *et al.*, Phys. Lett. B **658**, 203 (2008).
[8] D. Sohler *et al.*, Phys. Rev. C **66**, 054302 (2002).
[9] M. De Rydt *et al.*, Phys. Rev. C **81**, 034308 (2010).
[10] B. Bastin *et al.*, Phys. Rev. Lett. **99**, 022503 (2007).
[11] C. Force *et al.*, Phys. Rev. Lett. **105**, 102501 (2010).
[12] L. Gaudefroy *et al.*, Phys. Rev. Lett. **102**, 092501 (2009).
[13] E. Cauriera, F. Nowackia, and A. Povesb, Nucl. Phys. **A742**, 14 (2004).
[14] L. Gaudefroy, Phys. Rev. C **81**, 064329 (2010).
[15] D. Sohler *et al.*, Phys. Lett. B **703**, 417 (2011).
[16] M. Hass, E. Dafni, H. H. Bertschat, C. Broude, F. D. Davidovsky, G. Goldring, and P. M. S. Lesser, Nucl. Phys. **A414**, 316 (1984).
[17] G. Neyens, Rep. Prog. Phys. **66**, 633 (2003).
[18] W.-D. Schmidt-Ott *et al.*, Z. Phys. A **350**, 215 (1994).
[19] G. Georgiev *et al.*, J. Phys. G **28**, 2993 (2002).
[20] I. Matea *et al.*, Phys. Rev. Lett. **93**, 142503 (2004).
[21] N. Vermeulen *et al.*, Phys. Rev. C **75**, 051302(R) (2007).
[22] T. Kubo, Nucl. Instrum. Methods Phys. Res., Sect. B **97**, 204 (2003).
[23] M. Birkholz, J. Phys. Condens. Matter **4**, 6227 (1992).
[24] R. M. Steffen and K. Alder, in *The Electromagnetic Interaction in Nuclear Spectroscopy*, edited by W. D. Hamilton (North Holland, Amsterdam, 1975), Chaps. 12 and 13.
[25] P. Hohenberg and W. Kohn, Phys. Rev. **136**, B864 (1964).
[26] W. Kohn and L. J. Sham, Phys. Rev. **140**, A1133 (1965).
[27] S. Cottenier, *Density Functional Theory and the Family of (L)APW-Methods: A Step-by-Step Introduction* (Instituut voor Kern- en Stralingsfysica, KULeuven, Belgium, 2002), ISBN (freely available from http://www.wien2k.at/reg_user/textbooks).
[28] P. Blaha *et al.*, *WIEN2k, An Augmented Plane Wave + Local Orbitals Program for Calculating Crystal Properties* (Karlheinz Schwarz, Techn. Universitat Wien, Austria, 1999), ISBN .
[29] P. Dufek, P. Blaha, and K. Schwarz, Phys. Rev. Lett. **75**, 3545 (1995).
[30] L. Errico, G. Darriba, M. Rentería, Z. Tang, H. Emmerich, and S. Cottenier, Phys. Rev. B **77**, 195118 (2008).
[31] H. Haas and J. G. Correia, Hyperfine Interact. **198**, 133 (2010).
[32] Technical settings were: PBE functional, $R_{\mathrm{MT}}^{\mathrm{Fe}} = 2.05$ a.u., $R_{\mathrm{MT}}^{S} = 1.95$ a.u., $K_{\mathrm{max}} = 7.0/R_{\mathrm{MT}}^{\mathrm{min}} = 3.59$ a.u.$^{-1}$, 249 k points in the irreducible part of the Brillouin zone ($18 \times 18 \times 18$), experimental lattice parameter ($a_0 = 5.412$ Å) together with an *ab initio* determined S position ($x = 0.382\,67$).
[33] B. J. Evans, R. G. Johnson, F. E. Senftle, C. Blaine Cecil, and F. Dulong, Geochim. Cosmochim. Acta **46**, 761 (1982).
[34] E. Caurier, ANTOINE code, IReS, Strasbourg 1989-2002.
[35] E. Caurier and F. Nowacki, Acta Phys. Pol. B **30**, 705 (1999).
[36] F. Nowacki and A. Poves, Phys. Rev. C **79**, 014310 (2009).
[37] L. Gaudefroy *et al.*, Phys. Rev. C **78**, 034307 (2008).
[38] R. W. Ibbotson, T. Glasmacher, P. F. Mantica, and H. Scheit, Phys. Rev. C **59**, 642 (1999).
[39] L. A. Riley *et al.*, Phys. Rev. C **80**, 037305 (2009).